IEEE Photonics Journal
An IEEE Photonics Society Publication

Open Access

Analog Photonic Link With Tunable Optical Carrier to Sideband Ratio and Balanced Detection

Volume 9, Number 2, April 2017

Yongsheng Gao
Aijun Wen, *Senior Member, IEEE*
Zhengxue Peng
Zhaoyang Tu

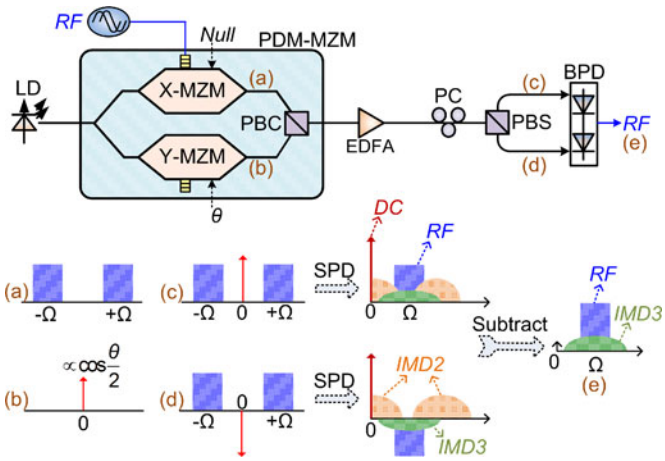

DOI: 10.1109/JPHOT.2017.2667891
1943-0655

Analog Photonic Link With Tunable Optical Carrier to Sideband Ratio and Balanced Detection

Yongsheng Gao,[1,2] Aijun Wen,[2,3] *Senior Member, IEEE*, Zhengxue Peng,[2,3] and Zhaoyang Tu[2,3]

[1]School of Electronics and Information, Northwestern Polytechnical University, Xi'an 710072, China
[2]State Key Laboratory of Integrated Service Networks, Xidian University, Xi'an 710071, China
[3]Collaborative Innovation Center of Information Sensing and Understanding, Xidian University, Xi'an 710071, China

DOI:10.1109/JPHOT.2017.2667891

Manuscript received December 20, 2016; revised February 5, 2017; accepted February 8, 2017. Date of publication February 15, 2017; date of current version March 1, 2017. This work was supported in part by the China 111 Project under Grant B08038 and in part by the National Natural Science Foundation of China under Grant 61306061 and Grant 61674119. Corresponding author: A. Wen (e-mail: ajwen@xidian.edu.cn).

Abstract: Optical carrier to sideband ratio (CSR) optimization and balanced detection are two effective techniques to improve the performance of an analogy photonic link (APL). Here, we proposed an APL where tunable optical CSR and balanced detection can both be implemented. A single integrated polarization division multiplexing Mach–Zehnder modulator (PDM-MZM) is used to generate a polarization multiplexed signal containing an optical carrier and two radio frequency modulated sidebands, and the optical CSR can be tuned from –15 to 15 dB by simply adjusting the direct current bias of the modulator. By optimizing the optical CSR in the proposed link, the link gain and noise figure (NF) are improved by 12 and 6.8 dB compared with conventional quadrature biased link. In addition, after balanced detection in the proposed link, the link gain, NF, third-order spurious free dynamic range (SFDR), and especially the second-order SFDR are further improved.

Index Terms: Analog photonic link (APL), balanced detection, carrier to sideband ratio (CSR), radio over fiber (RoF), spurious free dynamic range (SFDR).

1. Introduction

Thanks to the distinct advantages of large bandwidth, low loss, low weight, and immunity to electromagnetic interference, as compared with the radio frequency (RF) cable link [1], [2], the analog photonic link (APL) or radio over fiber (RoF) link has drawn much attention in modern electronic systems such as wideband wireless communications [3], satellite payload [4], radar [5], and electronic warfare systems [6]. However, the link gain, noise figure (NF) and spurious free dynamic range (SFDR) of an APL are often limited by the deficient modulation, strong noise, and nonlinear transfer function.

In a simple intensity-modulated APL, the modulator is conventionally operated at the quadrature point to suppress the second-order distortions. However, the low electro-optic modulation efficiency often leads to a huge optical carrier and relatively small sidebands or to, say, a large optical carrier

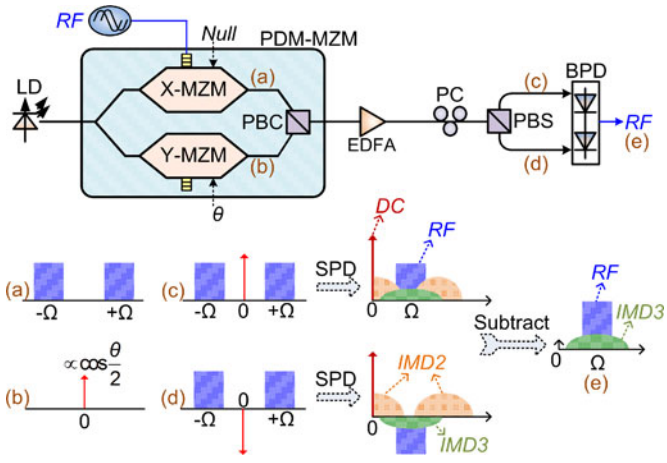

Fig. 1. Schematic of the proposed analog photonic link with tunable optical carrier to sideband ratio (CSR) and balanced detection. LD: laser diode; PDM-MZM: polarization division multiplexing Mach-Zehnder modulator; PBC: polarization beam combiner; RF: radio frequency; EDFA: erbium doped fiber amplifier; PC: polarization controller; PBS: polarization beam splitter; BPD: balanced photodiode. (a)–(e) Spectrum evolution of the optical and electrical signals.

to sideband ratio (CSR). The optical carrier contains no RF information and introduces much noise after photodetection, thus resulting in a high NF. The link gain and NF can be improved by injecting a large optical power to the photodiode [7], but limited by the optical power handling capacity of a commercial photodiode. Previous works reveal that a reduced optical CSR helps to optimize the link gain, NF and even the third-order SFDR ($SFDR_3$) [8]–[10]. The optical CSR can be reduced by low biasing [11]–[13], carrier filtering [9], [10], [14], or using parallel or cascaded modulators [15], [16]. However, these CSR optimization techniques will deteriorate the even-order linearity and second-order SFDR ($SFDR_2$), which is undesired in wideband or multi-carrier RF applications with multi-octave operation. To suppress the second-order intermodulation distortion (IMD2) in the low-biased APL, balanced detection is applied using Class-AB techniques [17]–[18]. In the intensity modulated Class-AB APL [17], the RF input signal is divided into two parts using a microwave power splitter and the two RF signals are applied to drive two parallel Mach-Zehnder modulators (MZMs), respectively. The two MZMs are low biased near but symmetrically about the null point, so two complementary optical signals are generated and the even-order components will cancel each other out after balanced detection. In [18], a Class-AB APL based on a polarization modulator, two polarization controllers (PCs) and two polarizers is also realized.

In this work, an APL with tunable optical CSR and balanced detection is proposed using a polarization division multiplexing Mach-Zehnder modulator (PDM-MZM). The optical CSR can be adjusted by tuning the direct current (DC) bias of the modulator. In addition, using a polarization beam splitter (PBS), two complementary optical signals can be generated for balanced detection. In the experiment, the optical signal with an optical CSR ranging from −15 to 15 dB is demonstrated. The link gain, NF and SFDR of conventional quadrature biased link and the proposed link with optical CSR optimization are measured and compared. Furthermore, balanced detection and optical CSR optimization are simultaneously realized in the proposed link, where the link gain, NF, and especially the $SFDR_2$, are significantly improved.

2. Principles

2.1 APL With Tunable Optical CSR

The schematic diagram of the proposed APL based on a PDM-MZM is shown in Fig. 1, which mainly contains a laser diode (LD), a PDM-MZM, an erbium doped fiber amplifier (EDFA), a PC, a

PBS and a balanced photodiode (BPD). The PDM-MZM integrates a Y-splitter, two dual-electrode sub-MZMs in parallel (X-MZM and Y-MZM), and a PBC [19].

Assuming the continuous-wave light wave output from the LD is expressed as $E_{in}(t) = E_c \exp(j\omega_c t)$, where E_c and ω_c are its amplitude and angular frequency, respectively. The light wave is power halved by the Y-splitter and sent to the two sub-MZMs. The RF signal, expressed as $V \sin(\Omega t)$, where V and Ω are the amplitude and angular frequencies, is applied to drive one RF electrode of the X-MZM. The X-MZM is biased at the null point to suppress the optical carrier, and the optical signal output from X-MZM can be expressed as

$$\begin{aligned} E_X(t) &= \frac{E_{in}(t)}{2\sqrt{2}} \{\exp[\, jm \sin(\Omega t)] - 1\} \\ &\approx \frac{E_{in}(t)}{4\sqrt{2}} \begin{Bmatrix} m[\exp(j\Omega t) - \exp(-j\Omega t)] \\ + \left(\frac{m}{2}\right)^2 [\exp(j2\Omega t) + \exp(-j2\Omega t)] \\ + \frac{1}{3}\left(\frac{m}{2}\right)^3 [\exp(j3\Omega t) - \exp(-j3\Omega t)] \end{Bmatrix} \end{aligned} \tag{1}$$

where $m = \pi V/(2V_\pi)$ is the modulation index, and V_π is the half-wave voltage of the modulator. The spectrum of the optical signal with only the $\pm$1st-order sidebands is illustrated in Fig. 1(a). The Y-MZM is only driven by the DC bias and generates an optical carrier expressed as

$$E_Y(t) = \frac{E_{in}(t)}{\sqrt{2}} \cos\frac{\theta}{2} \tag{2}$$

where θ is the bias phase shift and can be arbitrarily tuned to adjust the amplitude of the optical carrier, as shown in Fig. 1(b). The two optical signals are then combined by the PBC in the PDM-MZM and a polarization multiplexed signal with TE and TM modes expressed as below travels out of the PDM-MZM

$$E_{PDM-MZM}(t) = \vec{e}_{TE} \cdot E_X(t) + \vec{e}_{TM} \cdot E_Y(t). \tag{3}$$

The output polarization multiplexed signal is amplified by an EDFA with a power gain of G, adjusted by a PC, and then sent to the common port of a PBS. At each output port of the PBS, the two polarization modes of the optical signal are aligned to a single polarization mode. The optical filed at one output port of the PBS can be expressed as

$$\begin{aligned} E_1(t) &= \frac{1}{\sqrt{2}} [E_X(t)\cos\alpha + E_Y(t)\sin\alpha \exp(j\varphi)] \sqrt{G} \\ &= \frac{\sqrt{G}E_{in}(t)}{8} \begin{Bmatrix} \overbrace{4\cos\frac{\theta}{2}\sin\alpha\exp(j\varphi)}^{Carrier} \\ + \overbrace{m[\exp(j\Omega t) - \exp(-j\Omega t)]\cos\alpha}^{\pm 1st\ sidebands} \\ + \overbrace{\left(\frac{m}{2}\right)^2 \begin{bmatrix} \exp(j2\Omega t) \\ + \exp(-j2\Omega t) \end{bmatrix} \cos\alpha}^{\pm 2nd\ sidebands} \\ + \overbrace{\frac{1}{3}\left(\frac{m}{2}\right)^3 \begin{bmatrix} \exp(j3\Omega t) \\ - \exp(-j3\Omega t) \end{bmatrix} \cos\alpha}^{\pm 3rd\ sidebands} \end{Bmatrix} \end{aligned} \tag{4}$$

where α is the angle of the principal axes between the modulator and the output port of the PBS, and φ is the phase difference between the two polarization modes at the PBS, which can be both

tuned by the PC. The optical CSR in (4) can be easily calculated as

$$\mathrm{CSR} = 8\left(\cos\frac{\theta}{2}\tan\alpha/m\right)^2. \tag{5}$$

Note that the sideband power here refers to the total power of the ±1st-order sidebands. Given a specific modulation index, the optical CSR can be always tuned by the bias phase shift θ, or the polarization angle α.

2.2 Optical CSR Optimization

Here we assume the EDFA is working in an automatic power control (APC) mode and outputs a constant power of P_{EDFA}, which is close to the saturated power of the photodiode. According to (3), the average optical power output from the PDM-MZM can be expressed as

$$P_{PDM-MZM} = \frac{E_c^2}{16}\left(m^2 + 8\cos^2\frac{\theta}{2}\right) \tag{6}$$

where only the power of the optical carrier and the ±1st-order sidebands are calculated. The power gain of the EDFA can be calculated as

$$G = \frac{P_{EDFA}}{P_{PDM}} = \frac{16P_{EDFA}}{E_c^2\left(m^2 + 8\cos^2\frac{\theta}{2}\right)}. \tag{7}$$

Taking into (4), the photocurrent after a single photodiode (SPD) can be expressed as

$$\begin{aligned} i_1(t) &= \eta\left|E_1(t)\right|^2 \approx \frac{2\eta P_{EDFA}}{\left(m^2 + 8\cos^2\frac{\theta}{2}\right)} \\ &\cdot\left[\begin{array}{l} m\sin(2\alpha)\cos\dfrac{\theta}{2}\sin\varphi\sin(\Omega t) \\ +m^2\sin(2\alpha)\cos\dfrac{\theta}{2}\cos\varphi\cos(2\Omega t)/4 \\ +m^2\cos^2\alpha\sin^2(\Omega t)/2 + 2\cos^2\dfrac{\theta}{2}\sin^2\alpha \\ +m^3\sin(2\alpha)\cos\dfrac{\theta}{2}\sin\varphi\sin(3\Omega t)/24 \end{array}\right]. \end{aligned} \tag{8}$$

It can be seen that the photocurrent of the fundamental term at the frequency of Ω will be maximized when $\alpha = 45^0$, $\varphi = 90^0$, and $m = 2\sqrt{2}\cos\frac{\theta}{2}$, where the optical CSR equals to 1 (0 dB). The photocurrent can then be rewritten as

$$i_1(t) = \frac{1}{8}\eta P_{EDFA}\left[\begin{array}{l} \overbrace{2\sqrt{2}\sin(\Omega t)}^{Fundamental} - \overbrace{\cos(2\Omega t)}^{IMD2} + \overbrace{2}^{DC} \\ +\overbrace{m^2\sqrt{2}\sin(3\Omega t)/12}^{IMD3} \end{array}\right]. \tag{9}$$

2.3 Balanced Detection

The photocurrent expressed in (9) contains the fundamental, IMD2, DC and IMD3 terms, as shown in Fig. 1. The DC can be simply blocked. However, for a wideband multi-octave signal, the IMD2 terms may locate in the signal band and cannot be filtered out, which significantly limit the SFDR of the link. In the proposed link, balanced detection is applied to suppress the IMD2 terms.

The two output ports of the PBS have orthogonal principal axis; therefore, so the optical filed at the other output port is

$$E_2(t) = \frac{1}{\sqrt{2}}\left[E_X(t)\sin\alpha - E_Y(t)\cos\alpha\exp(j\varphi)\right]\sqrt{G}. \tag{10}$$

Taking $\alpha = 45^0$, $\varphi = 90^0$, and $m = 2\sqrt{2}\cos\frac{\theta}{2}$ into the calculation, the two optical signals at the output ports of the PBS become complementary, which is shown in Fig. 1(c)–(d). The photocurrent at the second output port of the PBS can be expressed as

$$i_2(t) = \frac{1}{8}\eta P_{EDFA}\left[\begin{array}{l}\overbrace{-2\sqrt{2}\sin(\Omega t)}^{Fundamental} - \overbrace{\cos(2\Omega t)}^{IMD2} + \overbrace{2}^{DC} \\ -\overbrace{\sqrt{2}m^2\sin(3\Omega t)/12}^{IMD3}\end{array}\right]. \quad (11)$$

If a BPD is used, its output photocurrent can expressed as

$$\begin{aligned} i_{BPD}(t) &= i_1(t) - i_2(t) \\ &= \frac{1}{\sqrt{2}}\eta P_{EDFA}\left[\overbrace{\sin(\Omega t)}^{Fundamental} + \overbrace{m^2\sin(3\Omega t)/24}^{IMD3}\right] \end{aligned} \quad (12)$$

as shown in Fig. 1(e). The DC and IMD2 terms after BPD are canceled out and only the fundamental and IMD3 terms are left. In addition, compared with the SPD mode, the BPD will double the photocurrents of the fundamental and IMD3 terms and so 6-dB increase of the link gain and IMD3 are predicted.

3. Experiment Results and Discussion

3.1 Experimental Setup

A proof-of-concept experiment is carried out. A continuous-wave light wave with a wavelength of 1551.83 nm, an average power of 10 dBm and a relative intensity noise (RIN) of about −160 dB/Hz is generated from a distributed feedback LD and directly sent to a PDM-MZM (Fujitsu, FTM7980EDA). The half-wave voltage of the modulator is 3.5 V and the 3-dB bandwidth is 30 GHz. A 8-GHz sinusoidal RF signal is generated form a microwave signal generator (Rohde & Schwarz, SMW200A) and applied to drive the RF port of one sub-modulator (X-MZM) at the null point. The optical signal output from the PDM-MZM is sent to an EDFA for power amplification. The EDFA is working in the APC mode and has a constant output power of 9 dBm. A three-paddle PC is used to adjust the polarization state before the PBS. The two photodiodes in the BPD (Finisar, BPDV2150R) have a responsivity of about 0.6 A/W and a responsivity imbalance between 0.15 to 0.5 dB. The RF common mode rejection of the BPD is about 15 dB. The optical power received by each photodiode is 5 dBm. The optical signal before the photodiode and the detected electrical signal are measured by an optical spectrum analyzer and a signal analyzer (Rohde & Schwarz, FSW50).

3.2 Tunable Optical CSR

First, the tunable optical CSR is demonstrated. The power of the RF signal is 3 dBm, and the modulated optical sideband remains unchanged. By adjusting the DC bias of the Y-MZM, the power of the optical carrier is consequently tuned, thus changing the optical CSR. The obtained optical spectra with CSR ranging from −15 to 15 dB are shown in Fig. 2.

The optical CSR can also be changed by tuning the polarization angle before the PBS according to (5), and a wider CSR range can be predicted. For example, the CSR will be zero when $\alpha = 0$ and infinite when $\alpha = 90^\circ$.

3.3 Optical CSR Optimization and Performance Enhancement

The link performance with different optical CSR is then studied. In the initial experiment, the link is operated in the SPD mode by connecting only one input port of the BPD. The RF input power

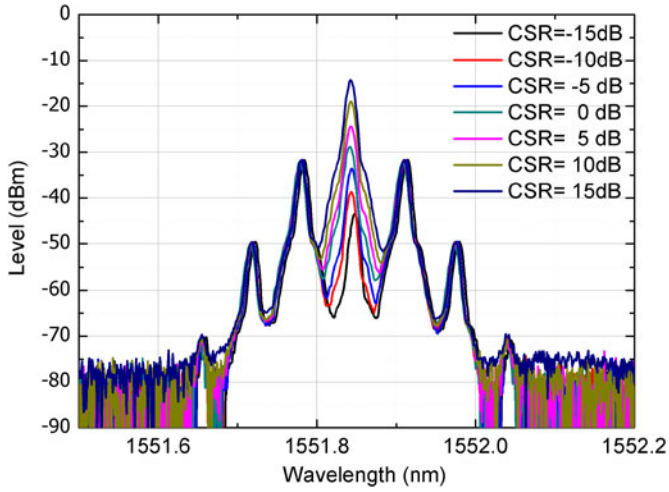

Fig. 2. Measured optical spectra with optical CSR ranging from –15 to 15 dB.

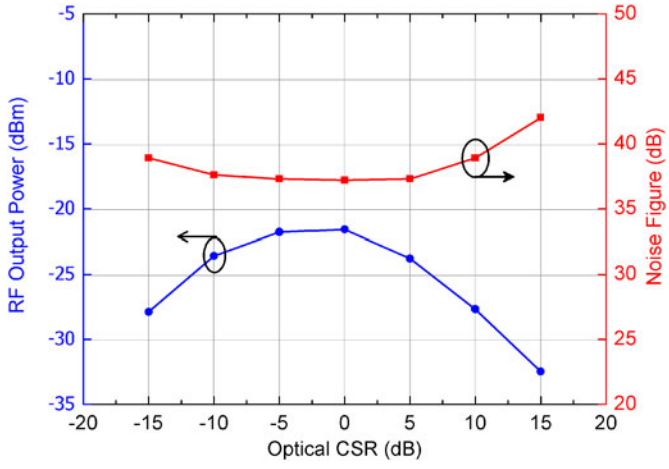

Fig. 3. Measured RF output power and noise figure with different optical CSR.

remains at 3 dBm and the RF output power as a function of the optical CSR is measured and shown in Fig. 3 using a blue line. The RF output power reaches its peak value when the optical CSR is 0 dB, which agrees well with the theoretical analysis. Meanwhile, the NF of the proposed link is also minimized when the optical CSR is 0 dB, which mainly benefits from the optimization of the RF output power.

Next, a two-tone signal at the frequency of 7.5 and 8 GHz is used as the RF input signal for intermodulation distortion analysis and SFDR measurement. By gradually changing the RF input power, the output power of the fundamental term, IMD2, IMD3 and noise floor are measured respectively. For comparison, the performance of a conventional quadrature biased APL based on an MZM is also measured and shown in Fig. 4(a). The MZM used here has a similar half-wave voltage with the PDM-MZM used in the proposed link, and the optical signals injecting the SPD in the two schemes are set to be equal in power. As can be seen from Fig. 4(a), the link gain and NF in the quadrature biased link are −32.2 and 43.6 dB, respectively. The measured $SFDR_2$ and the $SFDR_3$ are 93.1 dB·$Hz^{1/2}$ and 100.2 dB·$Hz^{2/3}$, respectively.

In the prosed PDM-MZM based link, where the optical CSR is optimized to 0 dB when the RF input power is 3 dBm, the measured results are shown in Fig. 4(b). The link gain and NF are

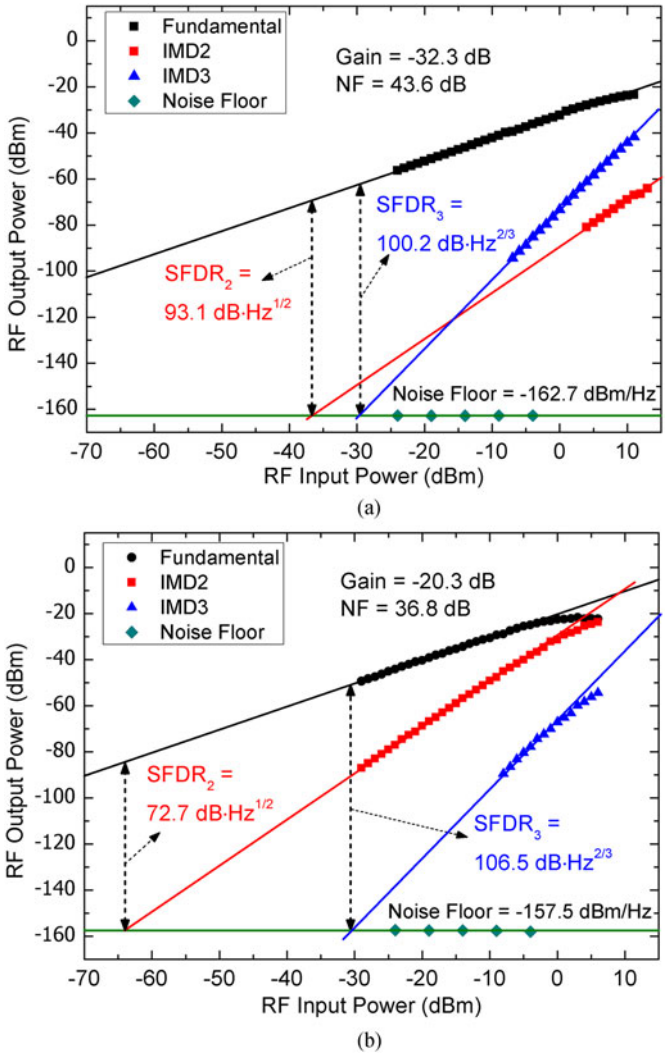

Fig. 4. Measured output powers of fundamental term, second-order intermodulation distortion (IMD2), third-order intermodulation distortion (IMD3) and noise floor as a function of the RF input power in (a) conventional quadrature biased link, and (b) proposed link after optical CSR optimization.

−20.3 and 36.8 dB, with 12- and 6.8-dB improvement, respectively. Meanwhile, the $SFDR_3$ is improved by 6.3 dB and reach 106.5 $dB{\cdot}Hz^{2/3}$. However, similar with other optical CSR optimization methods, the $SFDR_2$ in the proposed link is significantly deteriorated and is only 72.7 $dB{\cdot}Hz^{1/2}$, which is 20.4 dB lower than that in the quadrature biased link. In sub-octave applications where IMD2 can be simply filtered out, the proposed link after optical CSR optimization has a superior performance than the conventional quadrature biased link. In a multi-octave application; however, the IMD2 is always the dominant intermodulation distortion and seriously degrades the link performance.

3.4 Balanced Detection

To suppress the IMD2 in the proposed link, the link is then operated in the BPD mode according to Fig. 1. The two input ports of the BPD are connected to the two output ports of the PBS, respectively, and the PC before the PBS is carefully adjusted to generate two complementary optical signals for balanced detection.

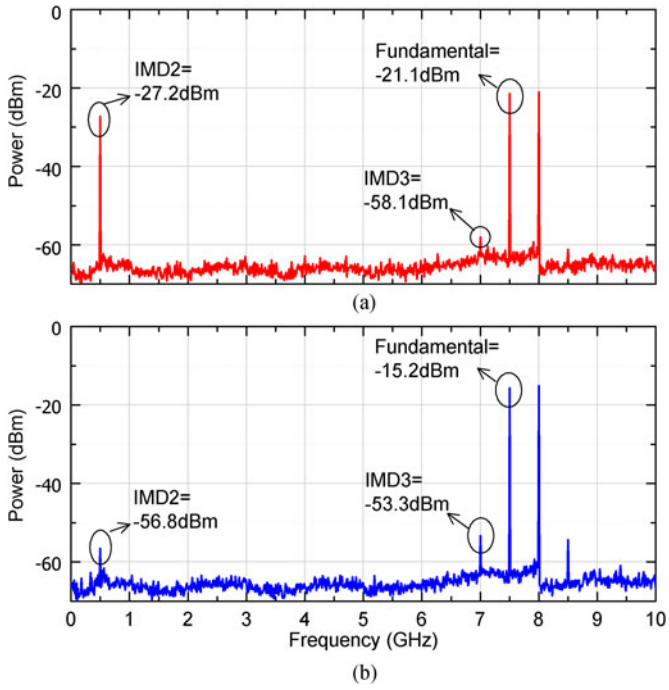

Fig. 5. Measured electrical spectra in the (a) single photodiode (SPD) mode and (b) balanced photodiode (BPD) mode.

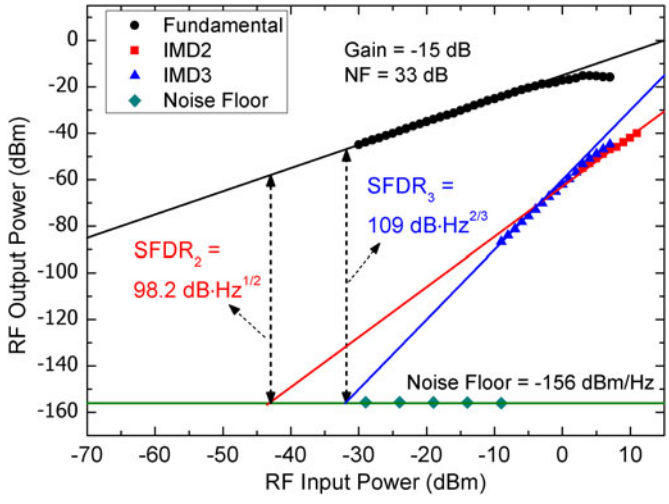

Fig. 6. Measured output powers of fundamental term, IMD2, IMD3, and noise floor as a function of the RF input power in the proposed link with optical carrier to sideband ratio optimization and balanced detection.

The electrical spectra in the SPD and BPD modes are shown in Fig. 5(a) and (b). As can be seen from Fig. 5(a), a large IMD2 at 0.5 GHz is observed, which is consistent with the result in Fig. 4(b). After balanced detection, as shown Fig. 5(b), the IMD2 is significantly suppressed by 29.6 dB. We can also see that the fundamental term at 7.5 or 8 GHz and the IMD3 at 7 or 8.5 GHz increase by 5.9 and 4.8 dB, respectively.

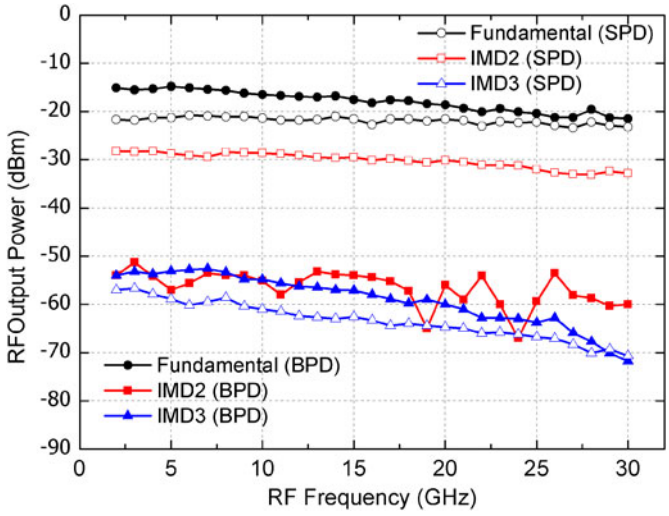

Fig. 7. Measured fundamental, IMD2, and IMD3 terms at different RF frequency in the SPD and BPD modes.

The link gain, NF and SFDR in the BPD mode are measured and shown in Fig. 6. In the theoretical analysis, the link gain may be improved by 6 dB after balanced detection. The measured link gain in Fig. 6 is −15 dB and 5.3 dB higher than that in Fig. 4(b), which basically agrees with the theoretical prediction. The system noise mainly comes from the laser RIN, shot noise and the EDFA introduced amplified spontaneous emission (ASE) noise [7]. The shot noise and ASE noise after the two photodiodes will be enhanced after balanced detection, while the RIN related noise originating from the same LD can be canceled. As a result, the system noise floor increases less than the link gain and so the measured NF is reduced to 33 dB after balanced detection. The measured $SFDR_3$ is 109 dB·$Hz^{2/3}$, where the 2.5-dB improvement mainly benefits from the 3.8-dB reduction of NF. Thanks to the suppression of IMD2 using the BPD, the $SFDR_2$ after balanced detection is as high as 98.2 dB·$Hz^{1/2}$, improved by 25.5 dB than that without balanced detection.

To further investigate the frequency tunability of the link, the frequency of the RF input signal is tuned from 2 to 30 GHz and the output fundamental term, IMD2, and IMD3 in the SPD and BPD modes are measured. As can be seen from the results shown in Fig. 7, the IMD2 after balanced detection is well suppressed over 20 dB in a wide frequency range from 2 to 30 GHz. In addition, the fundamental and IMD3 terms after balanced detection are improved in a wide band, basically consistent with the expectations. The relative power reduction of the fundamental term and IMD3 above 20 GHz may be due to the deterioration of responsivity imbalance and common mode rejection ratio (CMRR) of the BPD. Compared with other curves, the IMD2 curve in the BPD mode is much fluctuated with the working frequency, which is mainly due to polarization instability, the frequency-dependent responsivity imbalance and CMRR of the BPD.

In the experiment, if the single mode fibers (SMFs) between the modulator and the PBS are not touched and the temperature is not changed, the optical system is relatively stable. In practical applications, however, the external pressure on SMFs and the temperature variation may challenge the system stability. Except using polarization maintaining fibers (PMFs), a solution is to apply automatic polarization control techniques, which have been extensively explored and implemented previously [20]–[21].

4. Conclusion

An APL with a tunable optical CSR and balanced detection is proposed and experimentally verified using a PDM-MZM. By tuning the DC bias of the PDM-MZM, the power of the optical carrier can

be changed, thus adjusting the optical CSR. The tunable optical CSR can be used to optimize the link gain, NF and even the $SFDR_3$ of the APL. Experimental results reveal that the link gain, NF and $SFDR_3$ of the proposed link with an optical CSR of 0 dB are significantly superior to those in a conventional quadrature biased link. In addition, balanced detection is realized in the proposed link using a PBS and a BPD, and the link gain, NF, $SFDR_3$ and, especially, the $SFDR_2$ are further improved, making the proposed APL suitable for both sub-octave and multi-octave applications. As compared with the Class-AB link where the RF signal need to be divided to drive two symmetrical low biased MZMs, the proposed link also features the advantages of simple structure and easy implementation.

References

[1] R. W. Ridgway, C. L. Dohrman, and J. A. Conway, "Microwave photonics programs at DARPA," *J. Lightw. Technol.*, vol. 32, no. 20, pp. 3428–3439, Oct. 2014.

[2] J. Yao, "Microwave photonics," *J. Lightw. Technol.* vol. 27, no. 3, pp. 314–225, Feb. 2009.

[3] X. Li *et al.*, "Fiber-wireless-fiber link for 100-Gb/s PDM-QPSK signal transmission at W-Band," *IEEE Photon. Technol. Lett.*, vol. 26, no. 18, pp. 1825–1828, Sep. 2014.

[4] S. Pan *et al.*, "Satellite payloads pay off," *IEEE Microw. Mag.*, vol. 16, no. 8, pp. 61–73, Sep. 2015.

[5] S. Futatsumori, K. Morioka, A. Kohmura, K. Okada, and N. Yonemoto, "Experimental feasibility study of 96 GHz FMCW millimeter-wave radar based upon radio-over-fiber technology-fundamental radar reflector detection test on the Sendai airport surface," in *Proc. IEEE Int. Top. Meet. Microw. Photon.*, 2014, pp. 235–236.

[6] V. J. Urick, J. F. Diehl, C. E. Sunderman, J. D. McKinney, and K. J. Williams, "An optical technique for radio-frequency interference mitigation," *IEEE Photon. Technol. Lett.*, vol. 27, no. 12, pp. 1333–1336, Jun. 2015.

[7] D. A. I. Marpaung, *High Dynamic Range Analog Photonic Links: Design and Implementation.* Enschede, The Netherlands: *Univ. Twente*, 2009.

[8] R. A. Griffin, P. M. Lane, and J. J. O'Reilly, "Optical amplifier noise figure reduction for optical single-sideband signals," *J. Lightw. Technol.*, vol. 17, no. 10, pp. 1793–1796, Oct. 1999.

[9] J. Li *et al.*, "Performance analysis of an optical single sideband modulation approach with tunable optical carrier-to-sideband ratio," *Opt. Laser Technol.*, vol. 48, no. 11, pp. 210–215, Jun. 2013.

[10] C. Lim, M. Attygalle, A. Nirmalathas, D. Novak, and R. Waterhouse, "Analysis of optical carrier-to-sideband ratio for improving transmission performance in fiber–radio links," *IEEE Trans. Microw. Theory Tech.*, vol. 54, no. 5, pp. 2181–2187, May 2006.

[11] J. Devenport and A. Karim, "Optimization of an externally modulated RF photonic link," *Fiber Integr. Opt.*, vol. 27, no. 1, pp. 7–14, Jan. 2008.

[12] V. J. Urick, M. E. Godinez, P. S. Devgan, J. D. Mckinney, and F. Bucholtz, "Analysis of an analog fiber-optic link employing a low-biased Mach–Zehnder modulator followed by an erbium-doped fiber amplifier," *J. Lightw. Technol.*, vol. 27, no. 12, pp. 2013–2019, Jun. 2009.

[13] Y. Gao, A. Wen, J. Cao, Y. Chen, and H. Zhang, "Linearization of an analog photonic link based on chirp modulation and fiber dispersion," *J. Opt.*, vol. 17, no. 3, Feb. 2015, Art. no. 035705.

[14] Y. Gao, A. Wen, Y. Chen, H. Zhang, and S. Xiang, "Linearization of an intensity-modulated analog photonic link using an FBG and a dispersive fiber," *Opt. Commun.*, vol. 338, pp. 1–6, Mar. 2015.

[15] B. Hraimel, "Optical single-sideband modulation with tunable optical carrier to sideband ratio in radio over fiber systems," *J. Lightw. Technol.*, vol. 29, no. 5, pp. 775–781, Mar. 2011.

[16] Y. Zhang, F. Zhang, and S. Pan, "Optical single sideband modulation with tunable optical carrier-to-sideband ratio," *IEEE Photon. Technol. Lett.*, vol. 26, no. 7, pp. 653–655, Apr. 2014.

[17] T. E. Darcie and P. F. Driessen, "Class-AB techniques for high-dynamic-range microwave-photonic links," *IEEE Photon. Technol. Lett.*, vol. 18, no. 8, pp. 929–931, Apr. 2006.

[18] J. D. Bull, T. E. Darcie, J. Zhang, H. Kato, and N. A. F. Jaeger, "Broadband class-AB microwave-photonic link using polarization modulation," *IEEE Photon. Technol. Lett.*, vol. 18, no. 9, pp. 1073–1075, May 2006.

[19] Y. Gao, A. Wen, Z. Tu, W. Zhang, and L. Lin, "Simultaneously photonic frequency downconversion, multichannel phase shifting, and IQ demodulation for wideband microwave signals," *Opt. Lett.*, vol. 41, no. 19, pp. 4484–4487, Oct. 2016.

[20] M. Martinelli, P. Martelli, and S. M. Pietralunga, "Polarization stabilization in optical communications systems," *J. Lightw. Technol.*, vol. 24, no. 11, pp. 4172–4183, Nov. 2006.

[21] M. Yagi, S. Satomi, and S. Ryu, "Field trial of 160-Gbit/s, polarization-division multiplexed RZ-DQPSK transmission system using automatic polarization control," in *Proc. IEEE Conf. Opt. Fiber Commun., Nat. Fiber Opt. Eng.*, 2008, Paper OThT7.